Precise relocation of earthquakes following the 15 June 1991 eruption of Mount Pinatubo (Philippines).

Jean Battaglia, C.H. Thurber, Jean-Luc Got, C.A. Rowe, R.A. White

Precise relocation of earthquakes following the 15 June 1991 eruption of Mount Pinatubo (Philippines)

Jean Battaglia,[1] Clifford H. Thurber,[1] Jean-Luc Got,[2] Charlotte A. Rowe,[1,3] and Randall A. White[4]

Received 24 December 2003; revised 6 April 2004; accepted 10 May 2004; published 2 July 2004.

[1] The 15 June 1991 climactic eruption of Mount Pinatubo (Philippines) was followed by intense seismicity that remained at a high level for several months. We located 10,839 events recorded between 1 July and mid-December 1991. In contrast to the preeruptive seismicity which was focused in two groups below the summit area, posteruptive events were widely distributed below and around the volcano. The classification of the events indicates the presence of several large multiplets, and the application of relative relocation techniques to the similar events by calculating high-precision delays between traces outlines a number of clear seismogenic structures. We used different methods to confirm the validity of our results; these tests indicate that reliable features can be detected with a small monitoring network. While the main cluster of activity can be attributed to an intrusive process starting from below the 15 June crater, the volcanic origin of the seismic activity in the other areas is more difficult to establish. Away from the summit, relocations define streaks or planes which are oriented predominantly southwest-northeast, with in several cases the presence of northwest-southeast conjugate structures. Most of the composite focal mechanisms that we could determine indicate predominantly strike-slip, right-lateral faulting. Our results indicate that most of the seismicity that occurred after the 15 June eruption is related to the east-west regional compressional stress field related to the subduction. We suggest that the regional stress field induces seismicity along new or preexisting faults in the medium surrounding the volcano where the stress field was locally disturbed by the volcanic eruption. *INDEX TERMS:* 7280 Seismology: Volcano seismology (8419); 7230 Seismology: Seismicity and seismotectonics; 7215 Seismology: Earthquake parameters; 8419 Volcanology: Eruption monitoring (7280); 8494 Volcanology: Instruments and techniques; *KEYWORDS:* tectonic seismicity, relocation technique, volcanic eruption

Citation: Battaglia, J., C. H. Thurber, J.-L. Got, C. A. Rowe, and R. A. White (2004), Precise relocation of earthquakes following the 15 June 1991 eruption of Mount Pinatubo (Philippines), *J. Geophys. Res.*, *109*, B07302, doi:10.1029/2003JB002959.

1. Introduction

1.1. Background

[2] Mount Pinatubo is a composite volcano situated in the central part of Luzon island in the Philippines. It is part of the Luzon volcanic arc which runs parallel to the west coast of the island and whose volcanism is related to the eastward dipping subduction of the South China Sea Plate beneath Luzon island. Pinatubo is located at the place where the Iba fault zone, an east-west oriented graben, intersects the Bataan lineament which extends roughly north-south and on which 27 vents and volcanoes are aligned across Luzon [*Wolfe and Self*, 1983]. Locally, the Maraunot fault trends N30°W on the northwest flank of the volcano and is probably an extension of the Iba fracture zone [*Delfin et al.*, 1996]. The presence of a major northeast-southwest lineament, called the Sacobia lineament, was noticed by *Newhall et al.* [1996] and *Jones and Newhall* [1996]. It bounds the north side of the Sacobia pyroclastic and alluvial fans, passes through the caldera formed during the 15 June 1991 explosion, and may continue southwest of it.

[3] After about 500 years without any major eruptive episode [*Newhall et al.*, 1996], the volcano woke up in mid-March 1991 with the occurrence of earthquakes felt by the population and, on 2 April, with steam explosions [*Wolfe and Hoblitt*, 1996] along a northeastern trending fracture subparallel to the Sacobia lineament. Following this early unrest, the recorded seismicity first included mainly volcano-tectonic events grouped in a single cluster located about 5 km northwest of the summit and 4–6 km below sea level [*Harlow et al.*, 1996]. About 2 weeks prior to the mid-June climactic eruption the activity shifted to a shallower cluster located below the summit, initiating a buildup in the seismic activity that led to the 15 June eruption. In addition to the tectonic activity, preeruptive

[1]Department of Geology and Geophysics, University of Wisconsin–Madison, Madison, Wisconsin, USA.
[2]LGIT, Université de Savoie, Le Bourget du Lac, France.
[3]Now at Los Alamos National Laboratory, Los Alamos, New Mexico, USA.
[4]U.S. Geological Survey, Menlo Park, California, USA.

0148-0227/04/2003JB002959$09.00

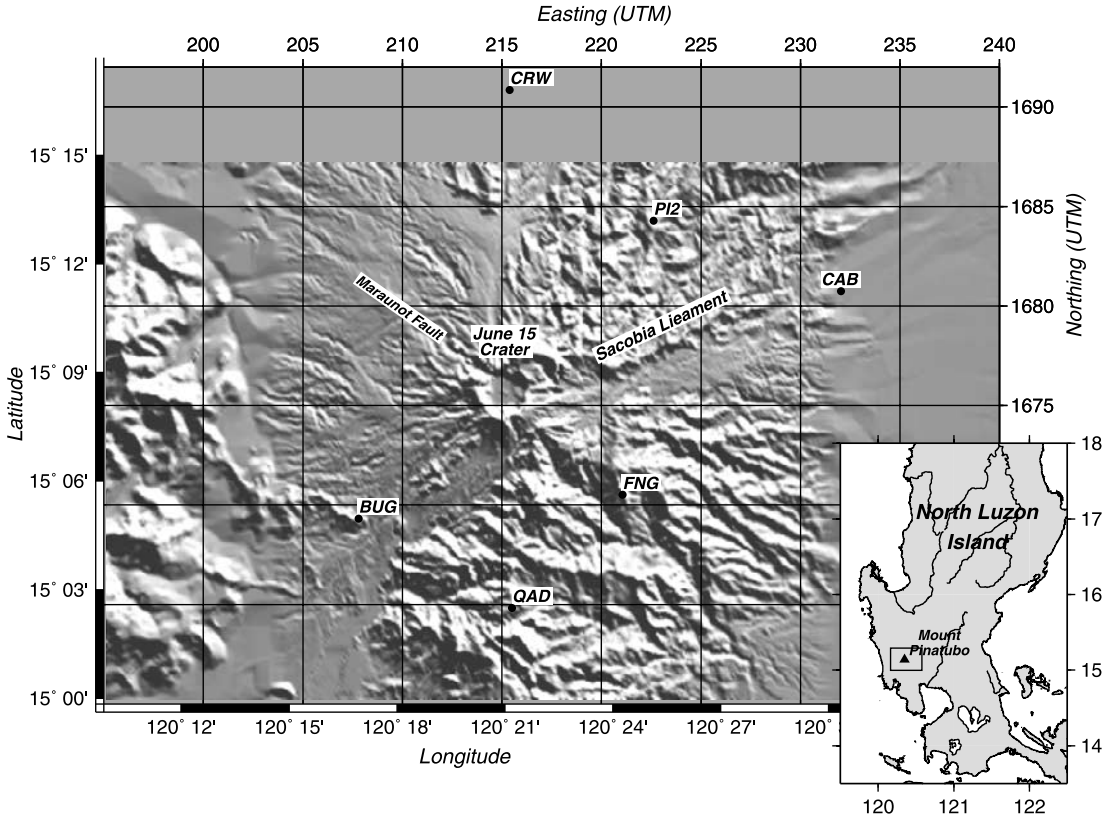

Figure 1. Shaded relief view of Mount Pinatubo plotted using a digital elevation model obtained after the 15 June 1991 eruption [*Jones and Newhall*, 1996]. Seismic stations used in the present study are shown as solid circles, and major lineaments are indicated. The location of the volcano is shown on the map of the northern part of Luzon island (Philippines) in the lower right corner of the plot.

seismicity included deep and shallow long-period (LP) events and tremor [*White*, 1996].

[4] The main 15 June eruption was followed by very intense volcano-tectonic activity which decayed rapidly over the first 2 weeks [*Mori et al.*, 1996b] but continued at a relatively high level for several months. Unfortunately, the first 2 weeks of posteruptive activity were only recorded by a single station situated at the Clark Air Base (CAB) since the remaining stations were destroyed on 15 June. Following the main explosion, the volcanic activity evolved from a continuous vigorous ash venting to a more intermittent explosive activity accompanied by bursts of increased low-frequency tremor. The activity slowed down by the end of July, and episodic ash emission continued until the beginning of September with a last reported explosion on 4 September. A detailed chronological summary of the seismicity and eruptive activity between 15 June and the beginning of September is presented by *Mori et al.* [1996b]. In addition to the low- frequency tremor and various seismic signals related to the ongoing eruptive activity, thousands of volcano-tectonic (VT) earthquakes were recorded during the waning eruption. In contrast to the preeruptive seismicity, the VT seismicity which followed the 15 June climactic eruption was distributed over a much wider area and depth range [*Mori et al.*, 1996a, 1996b; *Bautista et al.*, 1996] than the preeruptive one. The purpose of this paper is to study the VT activity recorded at this time to determine the characteristics of the seismogenic structures.

1.2. Earthquake Location Techniques

[5] Seismology is one of the most efficient techniques for gaining information about the internal structure and behavior of a volcano. The location of earthquakes permits the identification of active areas and allows the determination of their time evolution before, during, and after an eruption, providing information about the state of the volcano. However, the individual location of tectonic events by picking their arrival times manually or automatically generally yields a blurred image of the activity. Small errors in picking cause scattering of the locations, making the definition of clear structures and their interpretation difficult. This problem is worsened in the case of a network like that of Mount Pinatubo because of the small number of stations and the resulting poor constraints on the locations. In addition to the scattering of hypocenters caused by the inconsistency in phase picking and inhomogeneous observations, major sources of mislocation also arise from the poorly known velocity structure and the presence of velocity heterogeneities that affect travel times.

[6] Various techniques have been proposed to improve the location of earthquakes. Among these, a first main type of solutions is based on the improvement of the velocity model. The location programs commonly used

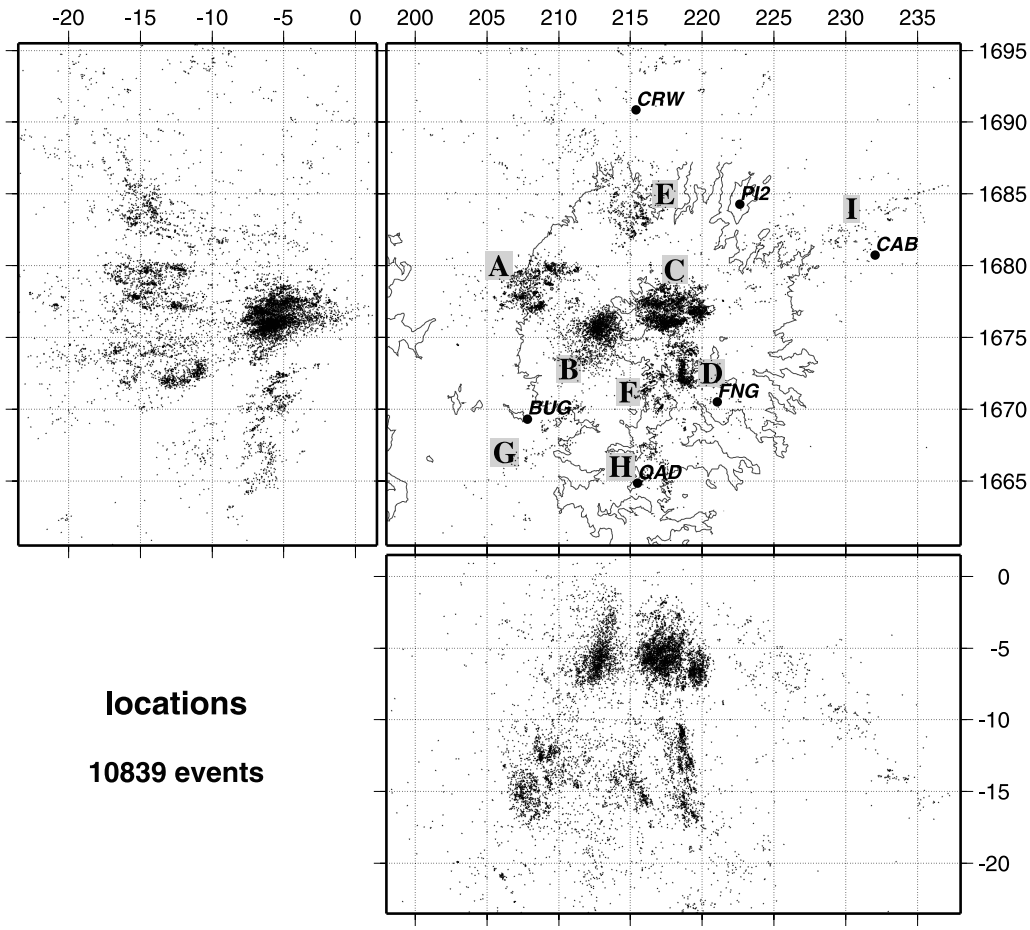

Figure 2. Map and cross sections showing the locations obtained with our "reference events" technique. Locations were obtained using a version of the simul2000 program which solves for locations and station corrections only, using the velocity model given in Table A1. The main clusters of activity discussed in the text are named A to I.

on a local or regional scale such as HYPO71 [*Lee and Lahr*, 1975] or HYPOINVERSE [*Klein*, 1978] use one-dimensional (1-D) velocity models with constant or gradient velocity layers. The determination of 3-D velocity models and the simultaneous adjustment of hypocenter locations provide a better knowledge of the velocity structure and allow the improvement of a large number of earthquake locations simultaneously. The 3-D structures thus obtained can then be used to improve the routine location of individual events using an appropriate location program [*Lomax et al.*, 2000]. The use of station corrections with a 1-D model [e.g., *Pujol*, 2000] is an alternate simple solution to partially account for lateral velocity variations.

[7] A second set of solutions is based on the use of arrival time differences for calculating the relative position of neighboring events. Rather than improving the velocity model, such techniques minimize the effects of the unknown velocity structure by using the arrival time differences to calculate the relative position between events. In particular, the use of waveform similarity allows the calculation of high-precision delays between trace pairs and provides high-precision relocations by also reducing the inconsistency in the picks. The presence of highly

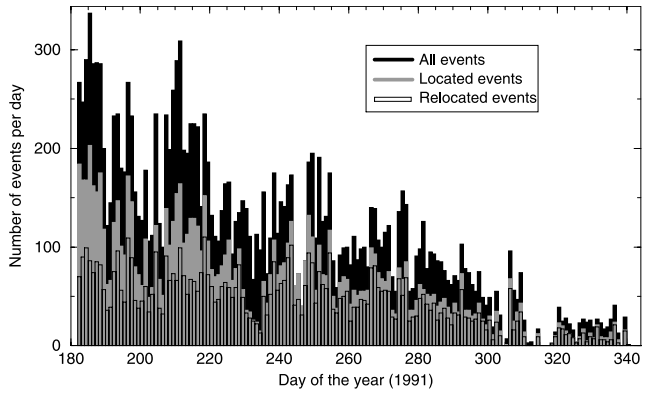

Figure 3. Number of events processed as a function of time at three different stages of our processing. "All events" are all the signals picked at station FNG, "located events" refers to the events we were able to locate using our "reference events" technique, and "relocated events" refers to the events we could group into multiplets and to which our precise relocation technique was applied.

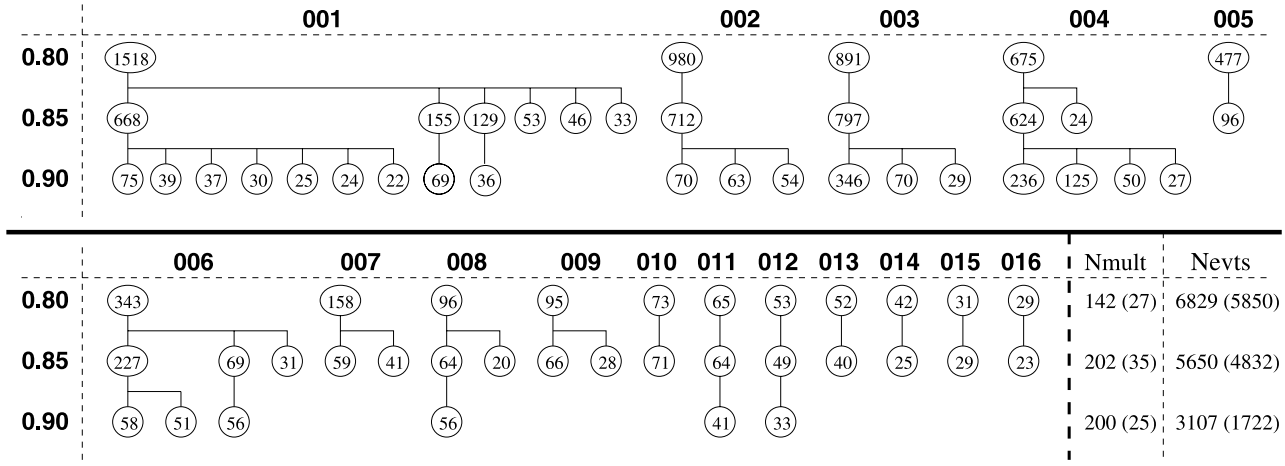

Figure 4. Number of events in the 16 largest multiplets (noted 001 to 016) as a function of the threshold used to define the similarity between the earthquakes. For example, 0.80 means that events are assumed to belong to a same multiplet if the cross correlation is higher than 0.80 at least at two stations of the network. Only subfamilies including more than 20 events are shown. The last two columns on the lower right show the number of multiplets (Nmult) grouping at least five events and the number of events (Nevts) grouped in those multiplets. In parentheses are the same quantities but for families of more than 20 events.

similar events, called multiplets, is a common feature and has been noticed at volcanoes like Usu [*Okada et al.*, 1981], Mount St. Helens [*Frémont and Malone*, 1987], Kilauea [*Got et al.*, 1994; *Wolfe et al.*, 2003; *Battaglia et al.*, 2003], Soufriere Hills, Montserrat [*Rowe et al.*, 2004], and Merapi [*Ratdomopurbo and Poupinet*, 1995] as well as in active tectonic regions like California [*Pechmann and Kanamori*, 1982; *Poupinet et al.*, 1984] and Japan [*Ito*, 1985]. The master event technique provides one solution for calculating the position of events relative to a single event. Such techniques have been used at Etna [*Brancato and Gresta*, 2003], Mount St. Helens [*Frémont and Malone*, 1987] as well in active tectonic areas as in Japan [*Ito*, 1985] and Europe [*Deichmann and Garcia-Fernandez*, 1992; *Scherbaum and Wendler*, 1986]. A more complete approach was provided by *Got et al.* [1994], who used time delays calculated for all possible event pairs of events within a family of similar events. This technique increases the relocation accuracy and does not imply the choice of a single reference event which has to be similar to all events in the multiplet. It has been shown to greatly sharpen the picture provided by the recorded seismicity [*Gillard et al.*, 1996; *Rubin et al.*, 1999, 1998; *Got and Okubo*, 2003]. More recently, the method was extended by *Waldhauser and Ellsworth* [2000] to allow the calculation of relative positions between nonsimilar events based on the use of catalog arrival times. Their algorithm hypoDD brings great improvements in the locations even by just using catalog arrival times [*Prejean et al.*, 2002], although the use of cross correlation delays provides further improvement of the earthquake locations.

[8] In this paper we use precise relocation techniques to study the seismicity recorded after the 15 June 1991 eruption of Mount Pinatubo. We first describe the precise relocation technique that we use. Because of the small number of stations available and related increased possibility of relocation errors, we discuss in detail a variety of methods to check the accuracy of the relocations. We finally present and discuss the results.

2. Data

[9] We use data from the local seismic network of the Pinatubo Volcano Observatory. The network was first installed by the Philippine Institute of Volcanology and Seismology and the U.S. Geological Survey in late April to early May 1991 to monitor the rewakening of Mount Pinatubo [*Lockhart et al.*, 1996]. This first network was, however, almost entirely destroyed during the main 15 June 1991 eruption and was restored with a different deployment geometry by the end of June 1991. In this paper we analyze the seismicity recorded from 1 July 1991 to 6 December 1991. For most of our study the network included six stations working properly; their locations are shown in Figure 1. All stations had short-period vertical seismometers with only one station (CAB) equipped with a single horizontal component.

[10] Triggered data were digitally recorded with a 100 Hz sampling frequency. For the 5 month period covered by our study, 17,586 recordings are available, with 10,538 triggered data files for July and August and only 1036 files for November–December. Many of the files include several earthquakes.

3. Relocation Method

[11] A preliminary step required to apply precise relative relocation techniques is to have initial absolute locations and the corresponding arrival times. Unfortunately, no catalog locations were available for our data, nor any reliable picks. In Appendix A we detail the technique which we used to pick 10,839 events. The preliminary locations obtained for those events are shown in Figure 2, and their temporal distribution is given in Figure 3.

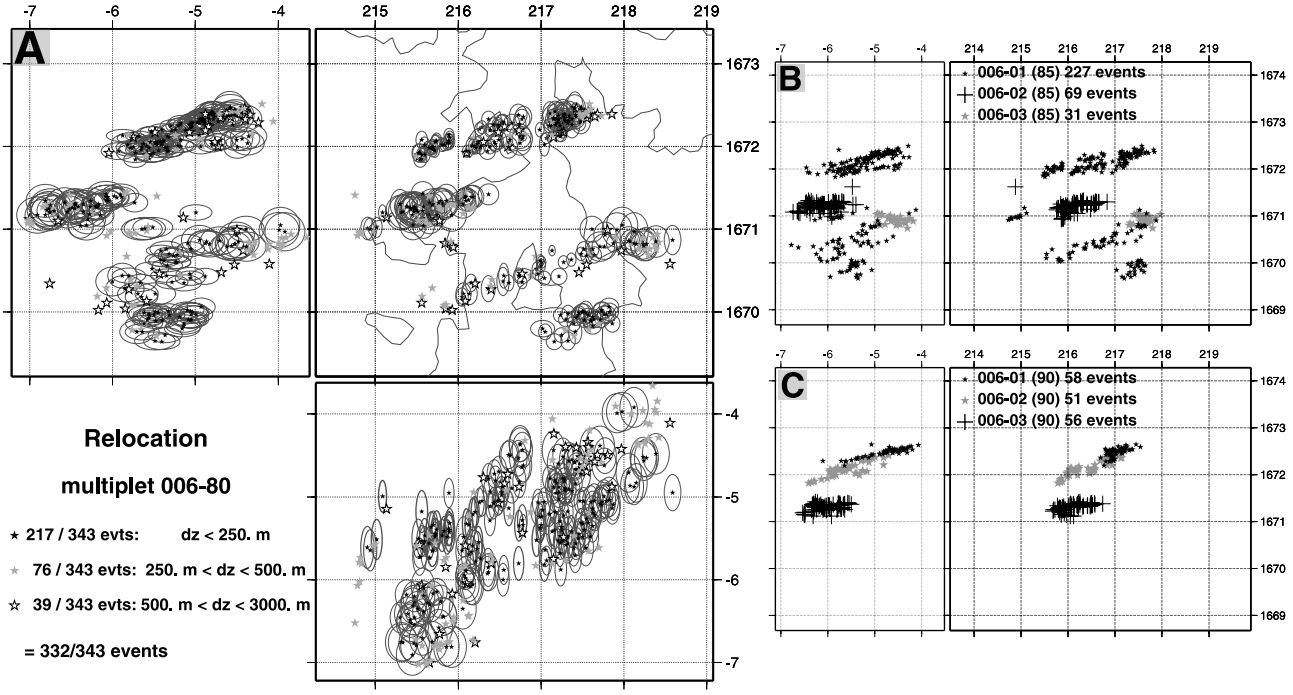

Figure 5. Tests to check the reliability of the relocations for problems related to poorly constrained relocations applied to multiplet 006. (a) Result for the relocation of the 343 events. Relocations are plotted with different symbols depending on their vertical uncertainty as described in the lower left corner of the plot. Error ellipses calculated using a Monte Carlo simulation are plotted for the 218 well constrained events only for purpose of clarity. (b) and (c) Relocations for three subfamilies of multiplet 006 at threshold $C_{\text{lim}} = 0.85$ (Figure 5b) and $C_{\text{lim}} = 0.90$ (Figure 5c).

[12] To calculate the precise relative positions of the events, we use the approach of *Got et al.* [1994]. The processing follows three steps: identification of families of similar events, calculation of time delays between all similar pairs, and computation of the relative positions of the events. For the classification and delay calculation we use 256-point windows (2.56 s) starting 50 points before the *P* wave picks obtained during the location process detailed above.

[13] To group similar events, we calculate the "similarity matrix" for all 10,839 available events. We estimate the similarity between each pair of events by calculating the mean cross correlation over measurements from all stations with a correlation higher than 0.8, with the constraint that at least two measurements are available. To limit the influence of noise such as the presence of low-frequency tremor, we band-pass filter the signals between 3 and 20 Hz. The number of events assigned to a multiplet depends on the criterion used for defining the similarity. We assume two events belong to the same multiplet if their mean correlation is greater than a threshold C_{lim}. A high value for C_{lim} such as 0.9 leads to the formation of small multiplets of very similar events. Such families are very efficient for defining small-scale features, but the relative positions of the small multiplets is then only defined by the preliminary locations and is thus poorly known. On the other hand, using a lower value for C_{lim}, such as 0.8, allows the definition of larger families and larger-scale structure by grouping small highly similar multiplets together and by improving the information about their relative positions. In exchange, a low threshold may lead to grouping nonsimilar events, increase the scattering, and lead to poor relocations, meaning that the results have to be carefully verified. In this work we try to link a maximum number of events in order to define the major structures. For this reason we will mainly present results for clusters defined with $C_{\text{lim}} = 0.80$ as a threshold and use families defined with $C_{\text{lim}} = 0.90$ and $C_{\text{lim}} = 0.85$ to check the validity of the obtained results.

[14] Figure 4 summarizes the results of the classification of the 10,839 available events depending on the threshold used for defining the similarity between the events. For $C_{\text{lim}} = 0.80$, 142 multiplets grouping more than five events can be defined, including a total of 6829 events whose time distribution is given in Figure 3. There are 5850 of those events grouped in only 27 multiplets including more than 20 events. In the following, we use the following notation: 006-01 (85) corresponds, for example, to the first subfamily (counted from the left in Figure 4) of multiplet 006 for $C_{\text{lim}} = 0.85$.

[15] For each multiplet we calculate delays for all pairs of similar events at all available stations. We first use the standard cross correlation, calculated using signals band-pass filtered between 3 and 20 Hz, to determine delays with a one-sample precision. If the correlation is higher than 0.85, we then use the cross-spectral analysis [*Jenkins and Watts*, 1968] to obtain subsample precision. We note that the use of relatively long (2.56 s) windows may cause alignments on *S* waves rather than on *P* waves for some stations where most of the energy is found in the *S* wave train. This leads to overestimations in the delays and consequently will stretch the extent of the relocations. On the other hand, the

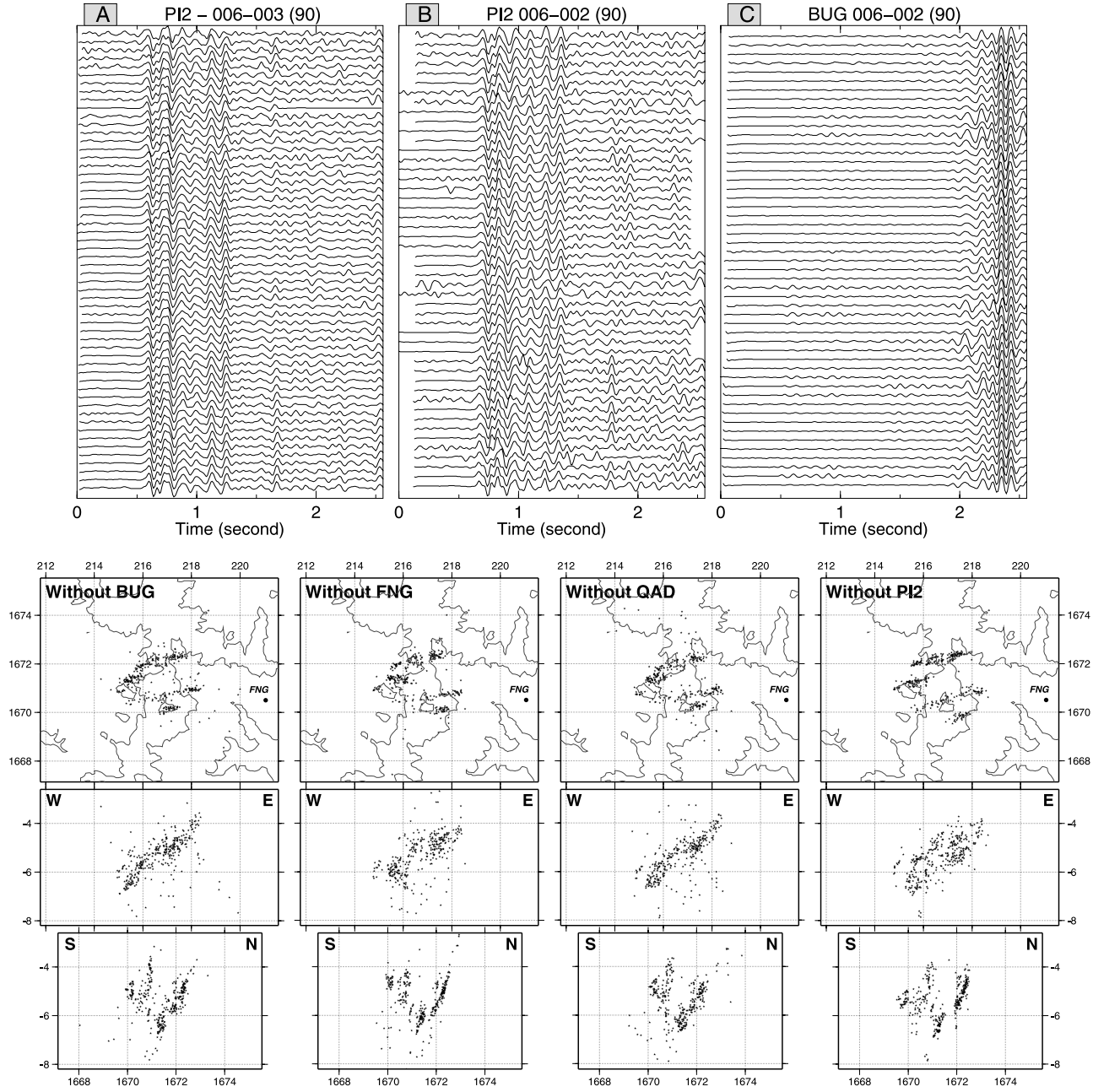

Figure 6. Tests to check the reliability of the relocations for problems related to wrongly constrained relocations applied to multiplet 006. (a) and (b) Alignments at station PI2 for two of the subfamilies (at threshold $C_{\text{lim}} = 0.9$) belonging to two different branches of multiplet 006. (c) Alignments at station BUG for one of those subfamilies when alignments are obtained on a later phase. The four bottom plots show examples of the application of the jackknifing technique. Each plot shows the result of the relocation when deleting one of the stations of the network: map view and E-W and N-S cross sections are shown.

use of such windows provides a major advantage as it allows reliable alignments for stations situated near *P* wave nodal planes and thus have very emergent onsets or even different onsets when on different sides of the nodal plane.

[16] Obtaining the relative position of the earthquakes is based on the assumption that the time delays only contain information related to the difference in the location of the events and thus can be linearly related to the corresponding relative source position vectors. This allows the problem to be formulated as a linear inverse problem and solved in a least squares sense. The use of delays calculated for all possible distinct event pairs leads the system to be strongly overdetermined and improves the accuracy of its least squares solution. A detailed explanation of the relocation process is given by *Got et al.* [1994]. In the processing, we use delays with a corresponding correlation value down to

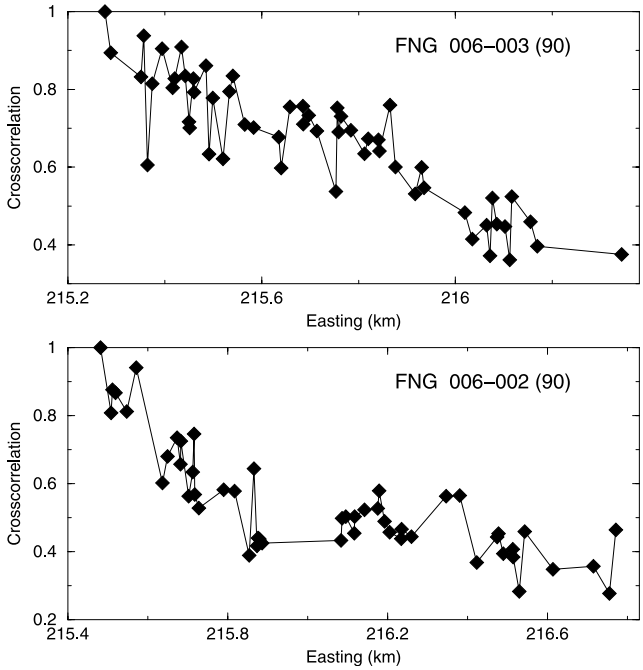

Figure 7. Test to check the self-consistency of the relocations applied to two subfamilies of multiplet 006. Plots show the correlation between the trace at station FNG for the most western event of each subfamily and traces for other events as a function of the easting. The correlation diminishes gradually, indicating loss of similarity as a function of distance, emphasizing the self-consistency of the lateral distribution of events.

0.5–0.6, since this provides more constraints, while erroneous delays (outliers) are rejected by appropriate statistical analysis [*Got et al.*, 1994]. The result of the relocation process is the position of the events relative to an arbitrary event in the multiplet, and the absolute geographic position of the relocated events is estimated by matching the centroid of the relocations with the geographic centroid of the corresponding initial locations.

4. Accuracy and Reliability of the Relocations

[17] Jointly relocating earthquakes usually improves their clustering and may also in some cases define specific shapes such as elongated patterns which could be interpreted as fault planes. It should be questioned, however, if these shapes are real or if they are an artifact of the relocation process. In particular, because of the small number of stations used in the present work the reliability and precision of the obtained relocations have to be examined carefully. We identify two main sources which may cause erroneously elongated patterns: (1) scattering of the relocations related to poor relocation constraints, and (2) poor waveform alignments at one particular station leading to an elongation in the direction of the station. In this section we present several techniques that we used to verify our results and illustrate their application using multiplet 006 and its subfamilies (Figure 4) as they show particularly interesting features.

[18] In the case of multiplet 006, all the different tests we present below indicate that the observed features are real. We, however, note that all tests cannot be applied successfully to each multiplet, and since no unique test could be found that brings conclusive results in each case, we present several different analysis techniques which we used to confirm our results. In addition to the tests presented below, we also compared our results for several multiplets with those provided by the software hypoDD [*Waldhauser and Ellsworth*, 2000] applied to the same set of cross-correlation delays, and the two techniques provide equivalent results.

4.1. Poorly Constrained Relocations

[19] The purpose of considering large families of similar events is to define larger-scale features. However, lowering the selection threshold for building families may cause scattering of the relocations due to the presence of poorly constrained events in the multiplets. An event linked to the rest of the multiplet by a small number of delays will be poorly constrained, as well as an event linked by a large number of delays for only a small number of stations.

[20] To define the uncertainty in each relocation, we use a Monte Carlo simulation assuming Gaussian errors on the takeoff and azimuth angles and on the delays. Uncertainties in x, y, and z are determined by running between 50 and 200 relocation processes (depending on the size of the multiplets) after introducing the Gaussian errors and calcu-

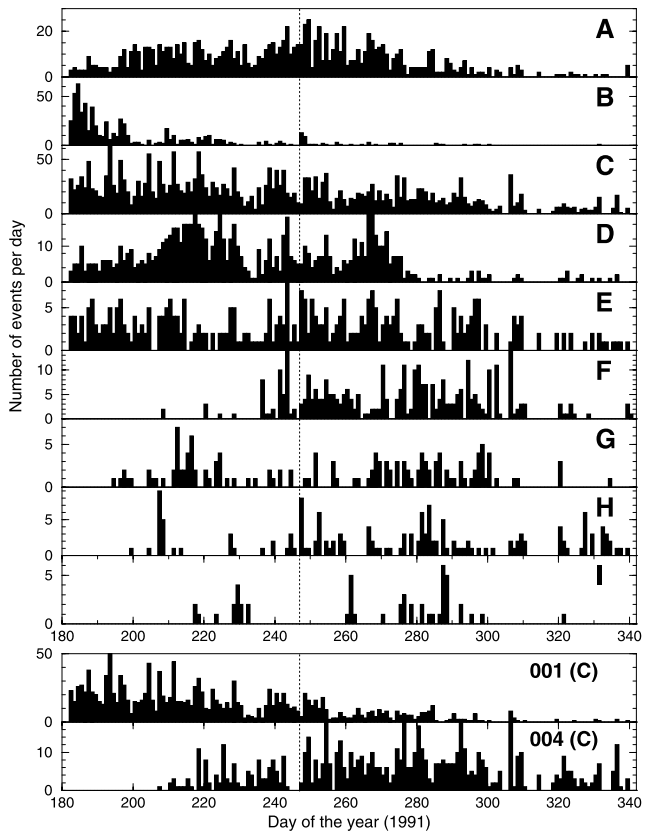

Figure 8. Histograms showing the number of events per day for each of the nine zones of activity denoted A to I. The time history for the two main multiplets (001 and 004) of zone C is detailed on the two bottom plots. The vertical dotted line indicates the date of the last observed explosion on 4 September (day 247).

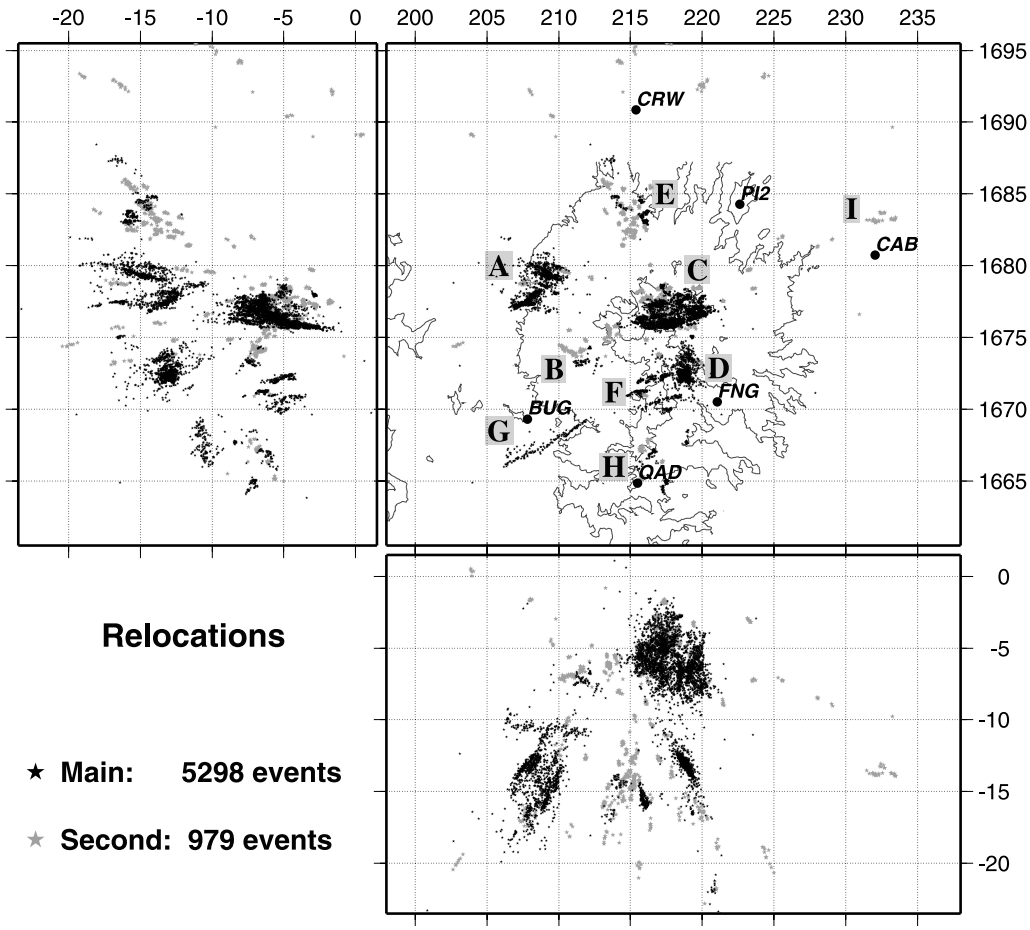

Figure 9. Relocations for all the multiplets. The 27 multiplets including more than 20 events (main) are shown as black, and the remaining ones (second) are shown as gray. Relocations for multiplet 005 (zone B), which mainly includes nontectonic events, are not shown.

lating the standard deviation over the results, which is used to draw approximate error ellipses. In the present work we assumed an uncertainty of 3° for the azimuth, 6° for the takeoff angle, and 7 ms for the delays. We note, however, that those values lead to large error ellipses in certain cases. The error estimates obtained are rather conservative. They are, for example, roughly 5 times larger than those obtained considering no uncertainties on azimuth and takeoff angles.

[21] Figure 5a shows the relocations obtained for the 343 events of multiplet 006. The error ellipses plotted for the 218 best constrained events show that the extension of the parallel planar features outlined by the relocations is far larger than the relocation uncertainty. In this example, most of the relocations with larger uncertainties fit into the features defined by the well constrained events and do not extend their size. Ten events with very large uncertainties are apparently improperly relocated.

[22] A complementary solution to verify the extension of the features is to look at subfamilies of more similar events. Highly similar events tend to be linked by an increased number of high-quality delays which reduces their scattering. Figures 5b and 5c show the results for the relocation of subfamilies of multiplet 006 at threshold $C_{\text{lim}} = 0.85$ and $C_{\text{lim}} = 0.90$. They indicate similar orientations and extension for the branches of multiplet 006, and most differences are caused by the poorly constrained relative position of the subfamilies.

4.2. Waveform Alignment Errors

[23] Having well-constrained relocations is unfortunately not sufficient to guarantee their accuracy. While for a large network the presence of a small number of erroneous delays will generally have little effect, in the case of a network of six stations, pick misalignment at one station may easily be the cause of bad relocations. Random misalignments distributed over the different stations will cause scattering, while persistent misalignment at a given station will cause elongated patterns in the direction of the station.

[24] A first approach to check for this problem is to visualize the trace alignments. However, this approach is only valid if it represents exactly the alignments used in the relocation process. The fact that delays between all pairs of events are used, rather than delays to a single master event, makes this task difficult. To visualize the alignments, we apply a procedure where the events are ordered according to their similarity using a dendrogram and offsets between traces are calculated starting from the most similar events. Examples of alignments obtained for two subfamilies of multiplet 006 are shown in Figure 6 for station PI2 as well as an alignment obtained at station

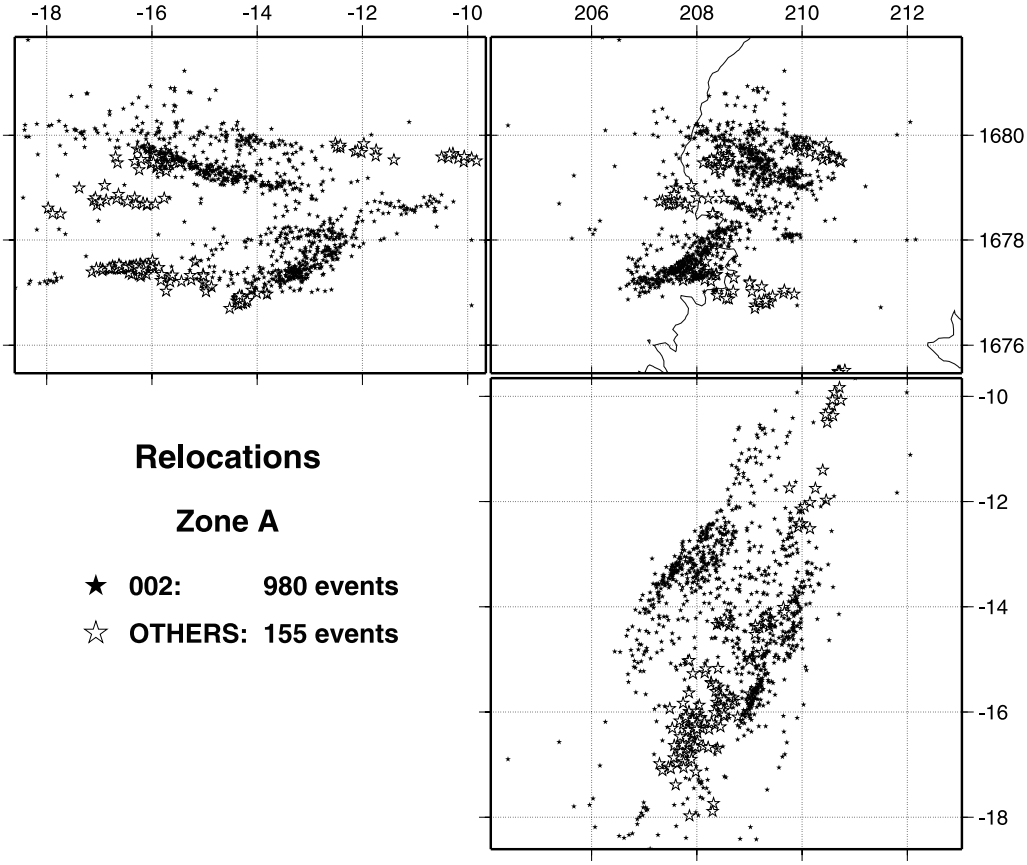

Figure 10. Relocations for multiplets in zone A. Different symbols are used to plot relocations for the main multiplet (002) and for the six smaller ones (OTHERS).

BUG using a later arrival phase for one of these subfamilies. Although these plots do not provide a complete view of the entire set of delays used for relocation, they yield insight into the waveform similarity and allow to rule out the presence of any major cycle skip. This technique is, however, difficult to apply to large families and events with a lower similarity.

[25] An alternate solution to check the influence of each station on the shape defined by the relocated events is to alternately remove one of the stations from the relocation procedure (jackknifing technique). Figure 6 shows examples of the application of this method to multiplet 006 when deleting stations BUG, FNG, QAD, and PI2 one at a time. The shape of the relocated events appears to be stable and not caused by only a single station. In particular, the removal of stations QAD and PI2, which control the north-south distribution of the events, indicates that the separation of multiplet 006 into several parallel branches is not caused by cycle skips between the traces of the different subfamilies. Despite the potential concern that deleting a station might lead to greatly increased location scatter, we instead find that the pattern of locations is generally quite robust for multiplet 006.

4.3. Proper Spatial Ordering of the Relocations

[26] Another approach to verify if elongated features defined by relocations are meaningful is to use some measure to check that the events are properly spatially distributed along the elongation axis and not just randomly. We may expect that the similarity between event waveforms will decrease as a function of the relative hypocentral distance, as the position of the station relative to the source radiation pattern changes and the seismic waves travel through increasingly different media. Then, for a cluster linearly extended in a given direction the similarity between an event at one tip and those located farther away should decrease as a function of the event separation. Figure 7 shows the correlation between the traces at station FNG for the most westerly event and those for other events as a function of the easting for two subfamilies of multiplet 006. The gradual decrease of the correlation with event separation for both subfamilies indicates that the events are properly ordered along the different branches of the multiplet.

5. Results

[27] Most of the seismicity that followed the 15 June eruption was focused in nine zones denoted A to I (Figure 2). In this section we describe the results of the relocation process for each zone and summarize the information about the activated seismogenic structures. The time and space distributions of the relocated events are shown in Figures 8 and 9, and relocations for selected individual zones are shown in Figures 10–14. Events which cannot be

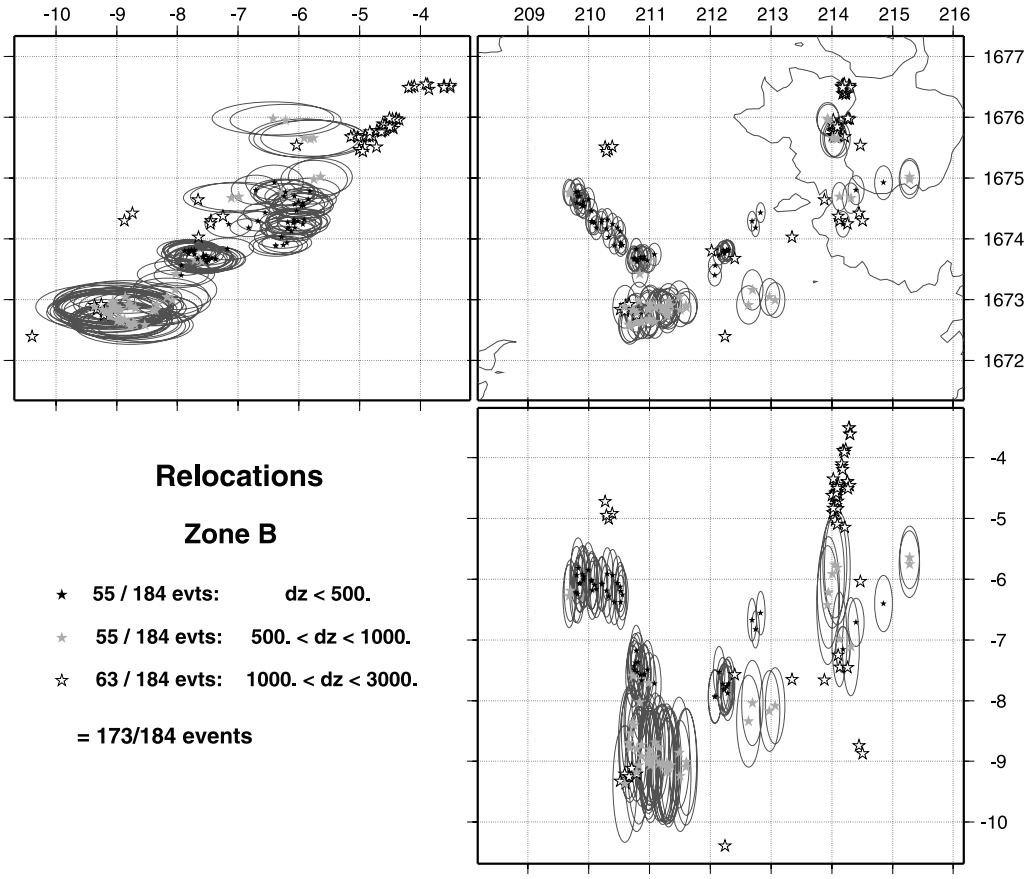

Figure 11. Relocations of all tectonic events found in zone B. Different symbols are used to plot relocations depending on their vertical uncertainty as described in the bottom left corner. Error ellipses are indicated for events with a vertical uncertainty lower than 1000 m.

relocated (orphans) are shown in Figure 15. We also present some focal mechanisms (Figure 16) whose calculation technique is detailed in Appendix B.

5.1. Zone A

[28] The area west of the summit is the site of the second largest family of similar earthquakes (002) with 980 events and also includes six smaller multiplets: a total of 1135 events (17% of the relocated events). The daily number of events in this area increased gradually until the end of explosive activity at the beginning of September and then decreased with the overall seismicity. Relocations in this zone are shown in Figure 10 and cover a rather broad area. For multiplet 002 the use of delays calculated with 2.56 s windows leads to unstable relocations because of the absence of stations to the west and cycle skips induced by the lowered frequency content of the signals related to the greater depth of the events. The use of 5.12 s signal windows greatly improves the quality of the relocations and emphasizes the presence of two distinct main branches with different orientations. The mean uncertainties obtained with the Monte Carlo method for events in the two branches are relatively low: 250 m for *X*, 130 m for *Y*, and 350 m for *Z*. The northern branch strikes 120° and has a predominantly vertical extension with a 65° dip to the north. This orientation is similar to that of the Maraunot fault which was mapped on the northwestern flank of Pinatubo [*Delfin et al.*, 1996]. The southern branch strikes 60° and dips 75° south. Several smaller streaks are also found in the area. We also note the rough alignment of the activity in zone A with that in zone C (north-south cross section in Figure 9).

5.2. Zone B

[29] Most of the events located in this area, about 95%, are nontectonic events and were recorded during July 1991 when the explosive activity was high, suggesting a tight link between the two phenomena. Their locations (Figure 2) delineate a vertical structure which could correspond to the lower part of the volcanic conduit below the eruption crater. We note, however, that these locations have very low quality and their vertical position is poorly constrained. The definition of a multiplet (005) among those events by our classification method is mainly due to the use of small signal windows and the dominantly low-frequency content of the signals. No accurate relocation was possible for these events. In addition to the nontectonic activity, 13 small multiplets of tectonic events, with only two families of more than 20 events, are found at the base of the column of nontectonic events. Their relocation with all the 184 events grouped into a single family is shown in Figure 11 and indicates the

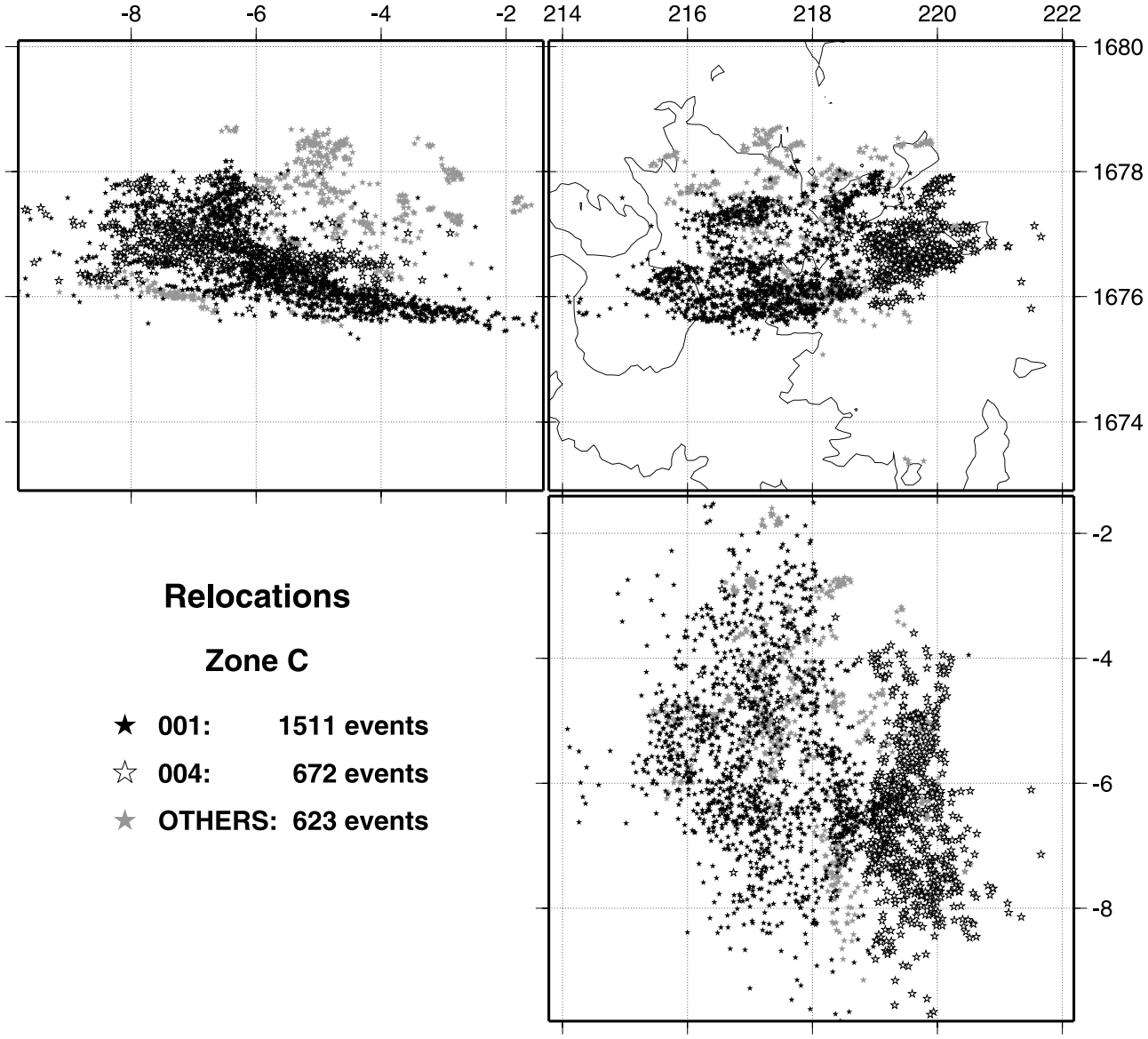

Figure 12. Relocations for multiplets in zone C. Different symbols are used to plot the two main multiplets which include 1511 (001) and 672 (004) events and the 47 smaller multiplets including at least five events (others).

presence of a couple of well-defined streaks with different orientations. Focal mechanisms were determined for the two main linear features (Figure 16) and indicate dominantly strike-slip motion along conjugate subvertical fault planes striking 70° and 135°.

5.3. Zone C

[30] The area situated east of the crater, below the summit, was the site of a very dense cluster of seismicity whose earthquake rate slowly decreased in time with an almost linear trend. In this cluster, 2806 of our relocated events are found which represents 41% of the relocated events and 26% of the entire set of located events. The 2806 earthquakes are grouped into 49 multiplets of more than five events, including 9 multiplets of more than 20 events. The two main families include 1518 (001) and 675 (004) events, respectively.

[31] The relocations for all multiplets found in zone C are shown in Figure 12. The main feature is the subvertical planar structure(s), dipping about 80° north, defined by the two main multiplets. It originates from the eastern side of the eruption crater and extends almost radially to the east. The western two thirds of the main planar structure correspond to multiplet 001 and are extended to the east by multiplet 004 which is rotated to the north by about 10–20°. North and at the bottom of the main plane are several linear branches. In particular, the branch centered at x = 218.7, y = 1677.5 and striking about 55° is well defined and includes highly similar events. The smaller multiplets are scattered mainly north of the main planar feature.

[32] For the two main multiplets the horizontal distribution of the events is well constrained with a mean uncertainty of about 200 m for X and 100 m for Y, and it

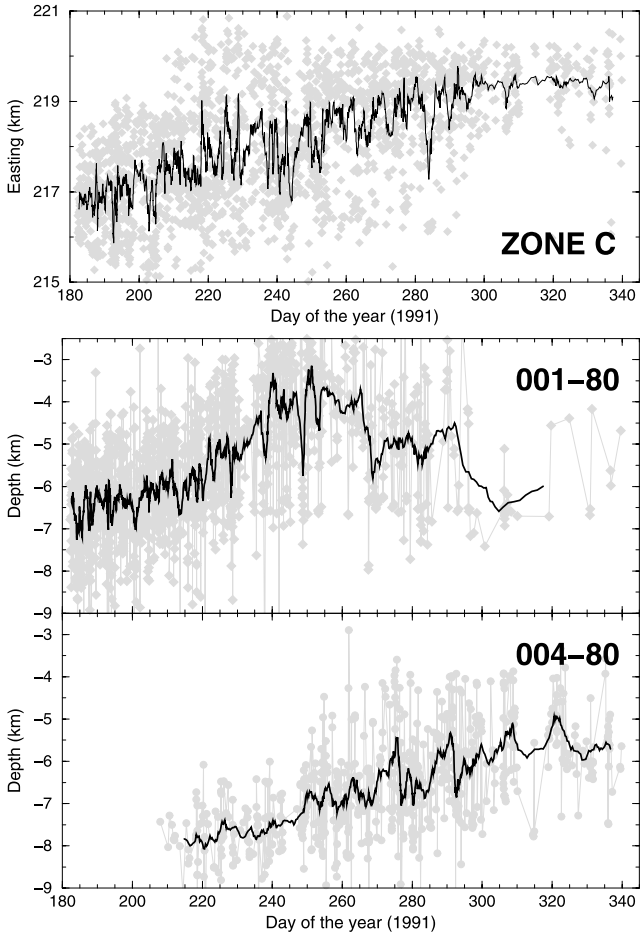

Figure 13. (top) Easting as a function of time for all events relocated in zone C. (middle and bottom) Depth as a function of time shown separately for relocated events in multiplets 001 and 004 which are part of zone C, respectively. On all plots, individual measurements are shown in background in gray, and the thick black line was obtained by averaging over 20-measurement windows.

is also stable to the jackknifing test. The vertical extent of the cluster is more difficult to confirm. The vertical uncertainty obtained with the Monte Carlo method has a mean value of about 600 m, is very low for events close to the vertical centroid of the cluster, and tends to increase for events situated away from it. The vertical extent of the cluster is, however, larger than those uncertainties, and a vertical extent of about 3 km is also indicated by relocations for higher similarity multiplets.

[33] Figure 13 shows easting as a function of time for all relocations in the area and the depth as a function of time individually for multiplets 001 and 004; all curves indicate striking migrations. The horizontal distribution shows an eastward migration of the hypocenters during the entire period of our study. This is also suggested by the fact that the activity shifts from multiplet 001 to 004 (situated more to the east) with time as shown in Figure 8. Multiplet 001 shows an upward migration of hypocenters from the beginning of July to about 5 September, which coincides with the end of explosive activity. After this period the migration tends to be downward. For multiplet 004 the activity starts later and indicates only an upward migration of the hypocenters until the beginning of December. We also note that the epicentral location of the events follows the surface expression of the Sacobia lineament (Figure 1) including its slight northward rotation as described by *Newhall et al.* [1996]. Focal mechanisms obtained for three subfamilies of both multiplets 001 and 004 indicate dominantly strike-slip right-lateral motion (Figure 16).

5.4. Zone D

[34] This zone includes mainly multiplet 003 (891 events, i.e., 13% of the relocated events) which collapses most of the events whose locations were scattered from 10 to 17 km depth along a branch-like pattern, into a small, mainly north-south elongated, plane (Figure 9) dipping about 65° to the east. Assuming that this plane corresponds to the fault plane, the focal mechanism obtained for events belonging to one of the subfamilies of multiplet 003 indicates predominantly normal faulting, in contrast to most of the other mechanisms that we obtained which mainly indicate strike-slip faulting (Figure 16). *Bautista et al.* [1996] suggested that this cluster could be related to the reactivation of a small portion of the old Tayawan caldera ring fracture. An alternate explanation is the activation of a small portion of the Bataan lineament which extends north-south through most of Luzon island.

5.5. Zone E

[35] The activity in zone E persisted during the whole duration of our study. Twenty-nine small multiplets are found in this area, with 6 of them having more than 20 events and the largest ones including 73 (010) and 53 (012) events. Despite the scattering related to the uncertainty in the relative position of the different multiplets, the relocations suggest the presence of two trends with streaks dipping to the east and some others dipping to the west (east-west cross section in Figure 9). Grouping all the events together and applying the relocation technique with a lowered threshold for similarity confirms the presence of an inverted V-shaped pattern as shown in Figure 14. The map view also outlines the presence of two branches striking about 48° and 140°. The error ellipses for the best relocations are relatively small and confirm both the shape and extent of the branches.

5.6. Zone F

[36] Most of the activity in this area happened after the end of August while the explosive activity was ending. Zone F is mainly the site of multiplet 006 whose processing was detailed previously. This multiplet emphasizes the presence of several parallel, well-constrained planar features striking 75° and dipping about 76° south at about 5 km below sea level. Focal mechanisms obtained for two subfamilies in the northern branch indicate predominantly right-lateral strike-slip motion (Figure 16). We note that if extended to the surface, the northern branch of multiplet 005 would intersect the surface close to the southern rim of the caldera which formed after the 15 June explosion, suggesting the possible activation of a portion of an outward dipping caldera ring fracture as

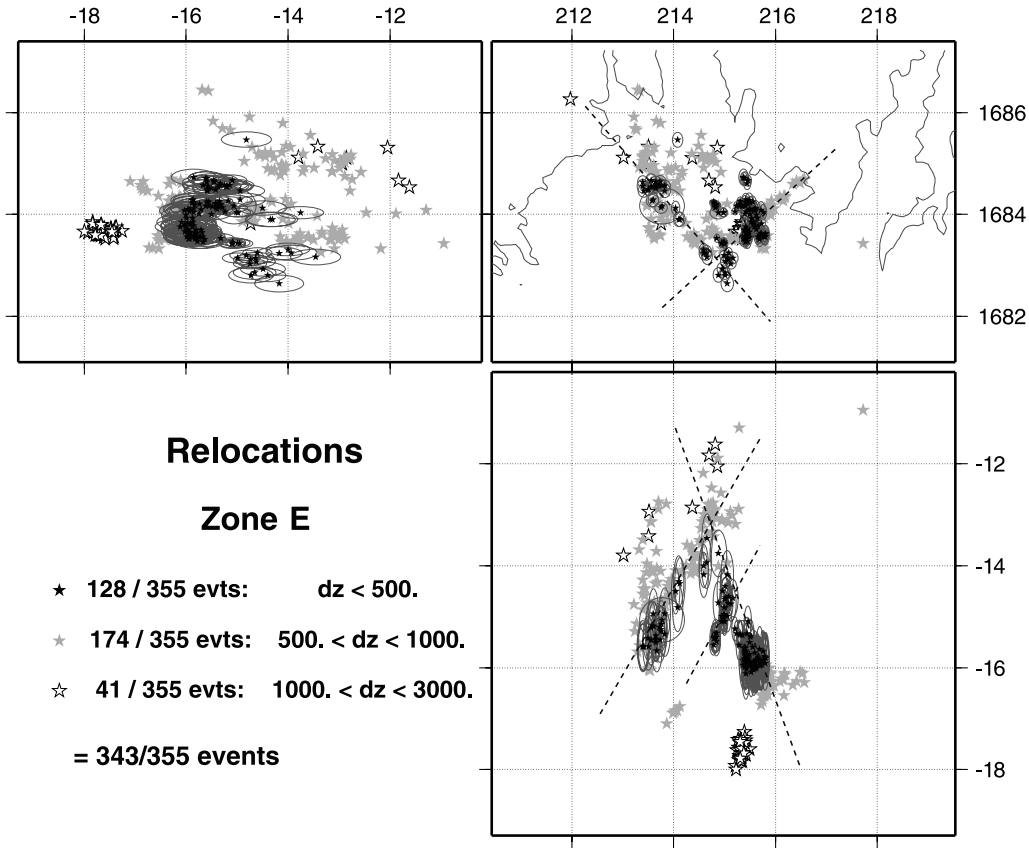

Figure 14. Relocations of all tectonic events found in zone E. Different symbols are used to plot relocations depending on their vertical uncertainty as described in the lower left corner. Error ellipses are indicated for events with a vertical uncertainty lower than 500 m.

observed at Rabaul caldera, Papua New Guinea [*Mori and McKee*, 1987]. An alternate and complementary explanation would be a readjustment of the southern flank of the volcano which includes several relatively large mountains (Mount Cuadrado, 1324 m, Mount Negron 1582 m) in response to the release of pressure below the summit in relation with the end of explosive activity. We, however, note that the focal mechanisms obtained along these structures are predominantly strike slip.

5.7. Zone G

[37] A single multiplet is found in zone G (007) and includes 158 events. The relocation of these events forms a linear feature which is well defined despite its situation at the edge of the network. Its spatial distribution is much larger than the uncertainty of the relocations, and the ordering of the events along the streak is meaningful according to the decrease of similarity. The epicentral location of the streak corresponds very well with a lineament striking 67° which appears in Figure 1, passing about 2 km southeast of station BUG and extending toward the southern edge of the crater. This lineament could correspond to an extension of the Sacobia lineament, offset by left-lateral motion along the Maraunot fault; the two features correspond to conjugate faults intersecting at the summit of the volcano. The focal mechanism obtained for this multiplet is shown in Figure 16 and indicates a predominantly right-lateral strike-slip mechanism.

5.8. Other Relocations and Orphans

[38] Zone H includes a total of only 153 relocated events divided into 6 small multiplets. Meaningful information is only provided by the relocation of one small group of 52 events which describes a small elongated pattern striking about 50°, north of station QAD. Other relocations in zone H collapse into small clouds. Zone I only includes small multiplets of less than 20 events which tend to be elongated in the east-west direction. Activity in zone I may correspond to the continuation of that in zone C, along the Sacobia lineament which passes north of station CAB. The interpretation of the relocations for most multiplets in zones H and I is made difficult by their position at the border of the network and poor resulting constraints. In addition to the previous main areas of activity, numerous small multiplets, often collapsing events into small streaks, are found mostly outside or close to the limits of the network.

[39] About 4560 of our locations, including nontectonic events, could not be grouped into multiplets according to our criteria (Figure 15). Generally, most of those orphans are located in the areas of activity described above and are probably part of the structures defined previously except that their similarity is not sufficient to satisfy our thresholds

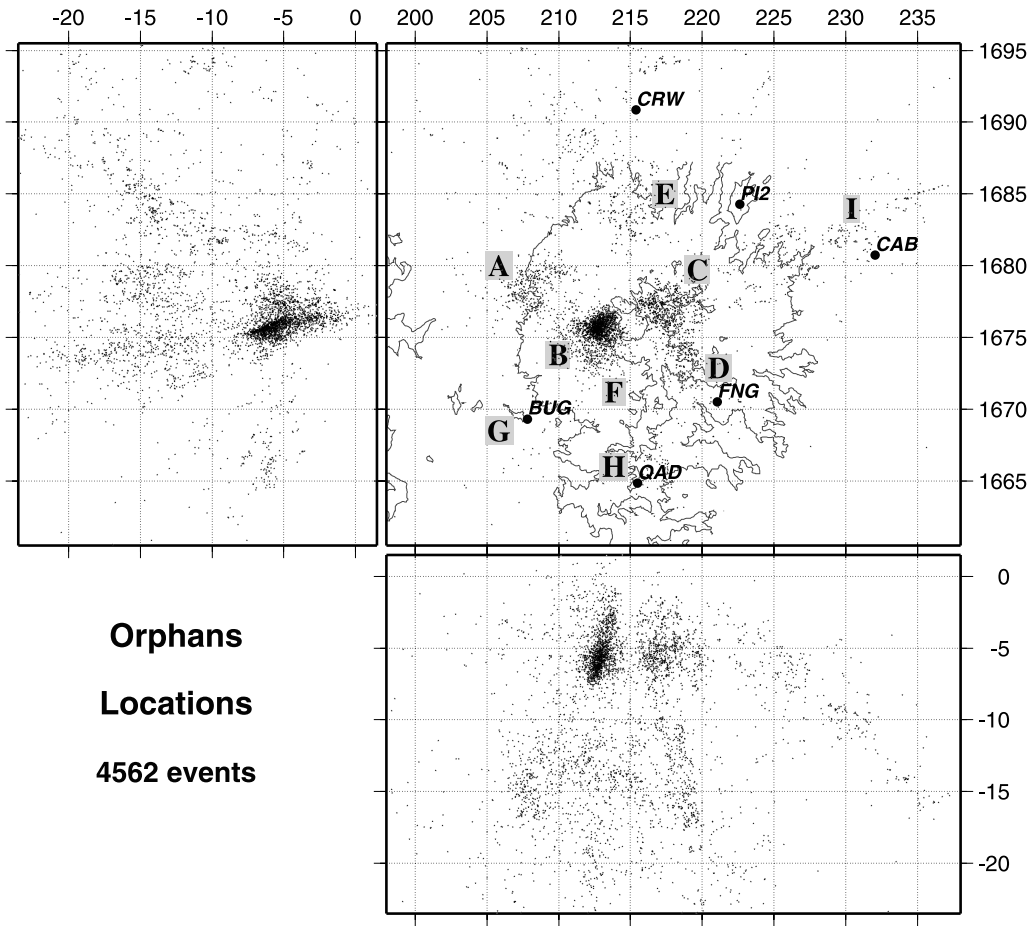

Figure 15. Locations for events which cannot be grouped into multiplets of more than five similar events (orphans).

and to allow precise relocations. In areas situated away from the summit a large part of the seismicity cannot be grouped into multiplets, largely because of the reduced similarity of traces at distant stations.

6. Discussion and Conclusion

[40] We located 10,839 seismic events recorded after the 15 June 1991 eruption of Mount Pinatubo. In contrast to the preeruptive seismicity which was mostly limited to two groups below the summit area, the locations for posteruptive seismicity are widely distributed below and around the volcano. Several main clusters of activity can be defined, most of them being away from the active volcanic center and/or deep. The classification of those events into families of similar events emphasizes the presence of several large multiplets. The application of relative relocation techniques to the similar events by calculating high-precision delays between traces outlines a number of clear seismogenic structures. These structures are usually streaks or planar features which can be interpreted as fault planes.

[41] There is an obvious concern that the small number of stations available (six) may be causing various artifacts in the relocation process, such as scattering due to poor constraints or elongated patterns caused by misalignments at one of the stations of the network. We used different methods to test the robustness of our results. Their application confirms the validity of our results and in particular it indicates that the shapes defined by our relocations are reliable. These results suggest that high-quality relocations can be obtained with a small network which is a common feature to a large number of monitored volcanoes.

[42] The main cluster of activity (zone C) is found east of the 15 June crater and accommodates 40% of the relocated events. Relocations define a vertically and almost east-west elongated planar feature which extends radially from below the crater. The migration of the hypocenters in this area, toward the surface and to the east, suggests a possible intrusive process along the Sacobia lineament. The inversion of the vertical migration from upward to downward by the beginning of September, when the explosive activity stopped, suggests the upward migration might have been driven by high pressure in the conduit which was also at the origin of the explosions. Focal mechanisms indicate, however, dominantly strike slip right-lateral faulting in this area.

[43] The direct relation between the seismic activity in the other areas and the volcanic activity and/or with the volcano plumbing system is more difficult to establish. Generally, it can be seen as the response of the brittle medium surrounding the volcano to the eruptive activity

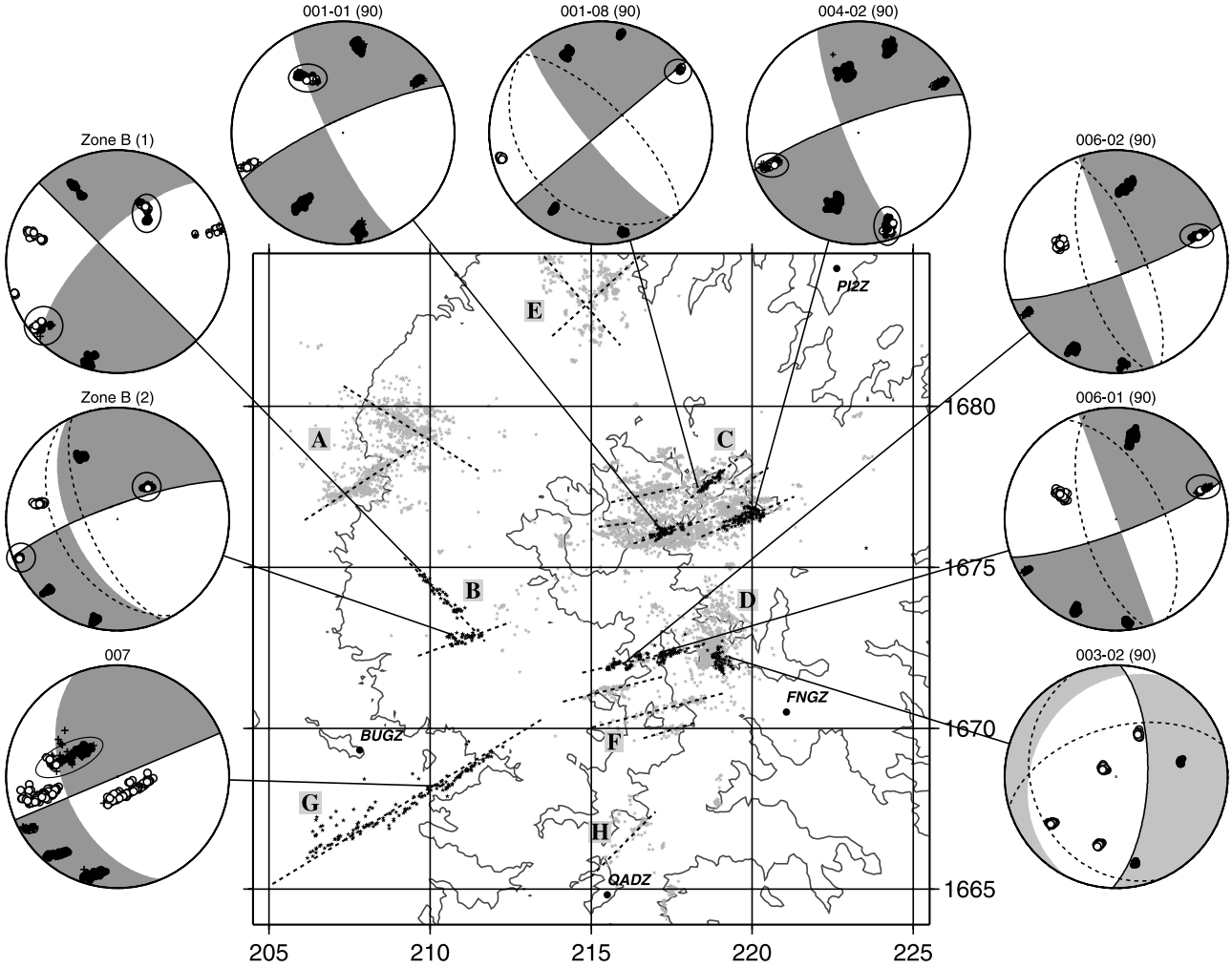

Figure 16. Composite focal mechanisms for several families of similar events. For each mechanism the nodal plane corresponding to the fault plane deduced from the relocations is indicated by a solid line. When an uncertainty remains on the position of the auxiliary nodal plane, limiting cases are drawn using dashed lines. Stations with both up (black circles, compression) and down (white circles, dilatation) first motions or very emergent *P* waves are circled. Events used for the determination of focal mechanisms are plotted as black stars on the map view of the volcano and superposed above the entire set of relocated events plotted in gray. Axes of several planar features or streaks are indicated using dashed lines.

and resulting stress changes. However, in detail, all clusters cannot be attributed to a common process of volcanic origin.

[44] Because of the removal of about 5 km^3 of material from below the volcano during the eruption and formation of a 2.5 km wide caldera on 15 June, we may expect a significant amount of the seismicity to be caused by caldera formation processes or more generally by the vertical collapse of the volcanic structure. Caldera formation was assumed to be at the origin of the strong seismicity observed in the case of other large eruptions at Fernandina volcano, Galapagos, in 1968 [*Filson et al.*, 1973] and Katmai volcano, Alaska, in 1912 [*Abe*, 1992]. In the case of Pinatubo, however, the seismicity does not clearly outline any circular structure that could be interpreted as a caldera as in Rabaul [*Mori and McKee*, 1987] or Campi Flegrei [*Troise et al.*, 1997]. Only a couple of clusters (zones D and F) can possibly be attributed to the activation of small portions of an outward dipping caldera ring fault formed on 15 June. A possible explanation for the absence of seismicity related to the caldera collapse is that most of it occurred during the first 15 days following the eruption when no records are available. An alternative is that most of the seismicity that accompanied the collapse had lowered frequency content similar to what was observed during a pit crater collapse at Piton de la Fournaise volcano [*Hirn et al.*, 1991]. Alternate and complementary origins for clusters D and F are the reactivation of a small portion(s) of a preexisting caldera ring fault (zone D) or the readjustment of the southern mountainous flank of the volcano (zone F).

[45] Another source of seismicity expected after an eruption is related to stress changes in the vicinity of the magma plumbing system. At Mount St. Helens, after the last 1986 eruption, the seismicity below the summit, in the 5–10 km depth range, surrounds an aseismic volume

which is interpreted as a magma chamber, with the earthquakes being caused by depressurization or repressurization of the active magma system [*Moran*, 1994; *Musumeci et al.*, 2002]. At Redoubt a cluster of deep (5–10 km) tectonic events was initiated below the summit by the eruptions on 15 December 1989 and is interpreted as being caused by the removal of magma from a source at that depth [*Power et al.*, 1994]. In some cases, stress changes caused by magma injections are at the origin of earthquakes very close to the intruding body, as, for example, in Hawaii [*Rubin et al.*, 1998] or below the Izu islands [*Toda et al.*, 2002; *Hayashi and Morita*, 2003]. At Mount Pinatubo the seismicity below the summit includes the main cluster of activity mentioned previously (zone C) and mostly nontectonic events (long-period events, explosion signals, tremor) whose locations are poorly constrained (zone B). Except for the possible intrusion in zone C, seismic activity does not clearly outline a well-defined magma system at depth. We note, however, that the seismicity below the summit only extends down to about 8 km depth. While deep clusters are observed away from the summit, no group is found below the summit, roughly defining the top of a wide low-seismicity zone whose limits are difficult to determine. The shallow depth of seismicity below the summit could indicate elevated temperatures that locally uplift the brittle-ductile transition as observed below Mount Spurr [*Jolly et al.*, 1994].

[46] Relocations for most of the clusters found away from the summit define streaks that are oriented predominantly southwest-northeast, within several cases the presence of northwest-southeast conjugate faults (Figure 16). These orientations are in good agreement with an east-west regional compressive stress field related to the subduction as suggested by *Acharya and Aggarwal* [1980], *Cardwell et al.* [1980], *Hamburger et al.* [1983], and *Bautista et al.* [1996]. Similarly, two distant clusters were also observed at depth following the major 1980 Mount St. Helens eruption [*Weaver et al.*, 1981] and were interpreted as being the crustal response to the release of seismic energy at the volcano, the *P* axis of those earthquakes being in good agreement with the compressional axis predicted by plate tectonics. We also note that like at Pinatubo, there was a major difference between preeruptive and posteruptive seismicity at Mount St. Helens.

[47] Closer to the summit, the orientation of the fault planes tends to rotate to a more east-west direction, reflecting the influence of the volcanic structure on the regional stress field. For most of the clusters the defined structures are outward dipping from the summit. Also, almost all of the focal mechanisms that we obtained indicate strike-slip, right-lateral faulting along those structures, including in the summit area. We note that *Bautista et al.* [1996] determined similar focal mechanisms for several clusters of earthquakes recorded during the same period of study as well as before the eruption. They also mention that the same type of focal mechanism was obtained using teleseismic recordings for several very large events (magnitude 4 and 5) that happened during the 15 June eruption. This suggests that some of the seismicity presented in this paper may correspond to aftershock sequences of those large earthquakes or those which occurred during the 15 following days, for which, unfortunately, no precise location is available. Overall, these results indicate that most of the seismicity that occurred after the 15 June eruption is related to the regional constraints. We suggest that the regional stress field induces seismicity along new or preexisting faults in the medium surrounding the volcano where the stress field was locally disturbed by the volcanic eruption.

Appendix A: Preliminary Location of Earthquakes

[48] Obtaining preliminary locations first requires picking the arrival times of earthquakes at the different stations of the network. Manual picking was excluded because of the extremely large number of events, and reliable automatic picking was made impossible by the commonly low signal-to-noise ratio, the frequent presence of several events in a single file, and the difficulty of automatically picking *S* waves at the only available horizontal component (recognizing that it provides an important constraint on the absolute location of the events).

[49] In order to pick the arrival times and to locate a maximum number of events we applied an iterative technique using a set of "reference events" manually picked to estimate arrival times for events not yet picked (called hereinafter referred to as test events). The method can be detailed as follows. To determine the complete set of available events, we first visualized all the available data for a single station (FNG) and picked the onsets of all events we could distinguish. Since it is often difficult to distinguish between the different types of events using a single station and to gain maximum information about the seismic activity, we also picked the onset of what appeared to be LP events or transients such as explosion signals. Station FNG was chosen as a reference because of its position close to the summit area and because it recorded most of the seismic activity. There were 16,863 signals selected this way, and the distribution of these events as a function of time is given in Figure 3. The preliminary picks thus obtained were used to extract 2.56 s windows (256 samples) at station FNG starting 50 samples before each pick.

[50] Our set of reference events was initially composed of about 400 randomly chosen events picked manually. Those events were augmented several times during the iterative process detailed below by choosing new reference events among the test ones. The selection of those events was done each time by calculating the matrix of cross-correlation values between traces at station FNG for all remaining test events and plotting dendrograms [*Everitt*, 1993]. We determined clusters of similar events according to the dendrograms and chose well-located reference events in each cluster. In this manner, we selected 595 additional reference events. Our final reference set of manually located events includes 681 events with seven picks available, 120 with six picks, and 194 events with five picks.

[51] The iterative process to pick the test events is done by first comparing them to the reference ones using cross correlation. For each test event we determine the closest neighbor (most similar event) among the reference ones. For those having a closest neighbor with a cross-correlation

Table A1. *P* Wave Velocity Model Used for the Location of Earthquakes

Depth, km	Velocity, km/s
−0.5	3.0
1.5	3.8
4.0	5.3
8.0	6.4
12.0	6.7
18.0	6.1
30.0	7.0

value higher than 0.75, we calculate delays for all stations between that neighbor's traces and those from the test event; delays with a very low cross-correlation value are not used. The arrival times are then recalculated for the test event using the obtained delays and its location is roughly determined using a 1-D velocity model given by *Mori et al.* [1996a] and the software HYPO71. If the result of the location has an RMS misfit lower than 0.15 s and if seven picks could be defined, the event is added to the reference set. Increasing the number of reference events allows the identification of better neighbors for events not yet processed or rejected during the previous rounds. The criterion about the number of picks required for moving a test event to the reference set was lowered to six and finally to five picks at later stages of processing. This process was repeated until no event could be moved from the test to the reference set. It finally led to a total of 10,067 events with at least five picks (6103 with seven picks, 2417 with six picks, and 1547 with five picks). There were 160 additional events picked using station CRW as a reference during periods when FNG was not working. The temporal distribution of the located events is given in Figure 3.

[52] A comparison of the signals collected at station FNG for the 6636 remaining events with each other indicated that no similar groups could be defined according to this station. A closer look at these remaining events indicates the presence of at least 1360 LP events, explosion signals, tremor onsets (referred to as nontectonic events), etc., recorded mainly during July and August 1991. Finally, we examined about 1097 events randomly chosen from the 5276 signals which could not be picked with our technique and were not clearly nontectonic: 485 "events" could not be located because they were not recorded by a sufficient number of stations, and 612 events were manually located. Among those 612 events, only poor quality locations could be obtained for 26% of them, and 45% occurred outside or at the periphery of the network, mainly close to stations CRW and CAB. This somewhat cursory analysis provides an estimate of what can be expected for the 4179 events that we did not locate. Most importantly, it did not identify the presence of any significant area of activity missed by our previous location process.

[53] In order to locate the events we use a 1-D velocity model with constant velocity gradients between interfaces (Table A1). This velocity model was obtained by inverting simultaneously the 1-D velocity structure, station corrections, and the locations of 3000 earthquakes distributed below the volcano using the code simul2000 [*Thurber and Eberhart-Phillips*, 1999]. The locations obtained for the 10,839 picked events are shown in Figure 2. Nine main areas of activity can be defined, denoted A to I. These locations include the different clusters of activity whose presence was noticed by previous studies [*Bautista et al.*, 1996; *Mori et al.*, 1996b], suggesting that our data set is representative of the entire seismic activity during the first months following the main 15 June eruption. Because our preliminary picking method is based on calculating delays relative to a set of reference events, the picking inconsistency is already greatly reduced and the clustering of the locations is improved as compared to classical individual locations.

Appendix B: Calculation of Focal Mechanisms

[54] In order to gain some information about the origin of the posteruptive seismicity we examined the focal mechanisms for several multiplets. Because of the small number of stations available we look at composite focal mechanisms by plotting the polarities of first motions for all events in a given multiplet rather than for individual events. For most of the multiplets, relocations define elongated patterns which we assume to correspond to the fault planes. We use this information to determine the azimuth and dip of one of the nodal planes. Then we look at the rake angles which give focal mechanisms that fit our first motion observations. Also, for several of the multiplets that we processed, first motions at some of the stations are very emergent, and both compressions and dilatations are observed. This suggests that those stations are close to the azimuth of one of the focal planes and confirms the orientations chosen for the fault plane and/or provides constraint on the position of the auxiliary plane.

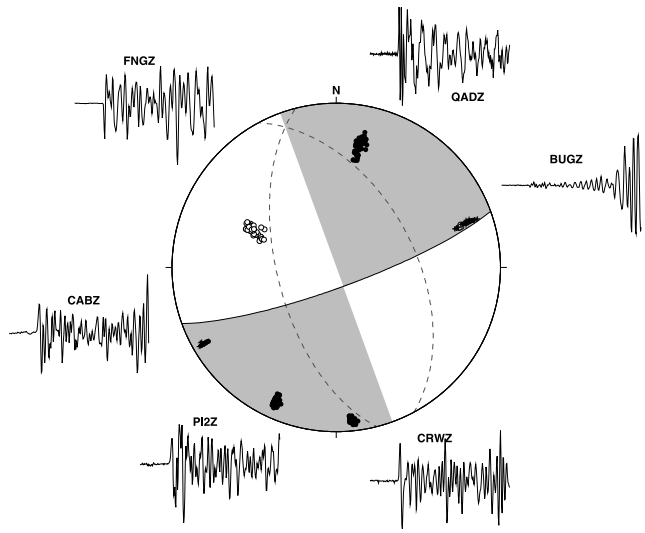

Figure B1. Composite focal mechanism for one of the subfamilies of multiplet 006 whose relocations are shown in Figures 5a and 5c (subfamily 006-01 (90)). Polarities of the first motions are indicated by black circles for compression and white circles for dilatation. Examples of seismic traces for the different stations are shown close to the corresponding first motions. The azimuth and the dip of the fault plane are defined according to the planar pattern defined by the relocations. The auxiliary plane was determined to fit the records, and the range of possible auxiliary planes is indicated by dashed lines.

We note that for these events the similarity of the traces at such stations is mainly on the later part of the signal and in the relocation process, delays are obtain by aligning those later phases. The spatial extent of the clusters and the polarity changes provide the justification for using composite instead of single-event mechanisms.

[55] An example of focal mechanism calculation is presented in Figure B1 for one of the subfamilies (006-01 (90)) of multiplet 006. Relocations shown in Figure 5a indicate a fault plane azimuth of about 70° and a dip of about 80° to the south. The orientation of the fault plane is confirmed by the fact that seismic traces at station BUG are very emergent and indicate both downward and upward first motions.

[56] **Acknowledgments.** We acknowledge the contributions of Director Raymundo S. Punongbayan (PHILVOCS) and Chris Newhall (USGS) for initiating the Pinatubo monitoring program, the USGS Volcano Disaster Assistance Program for providing most of the personnel and equipment for the initial seismic network installation and its posteruption replacement, the U.S. Office of Foreign Disaster Assistance for providing most of the funding, and PHIVOCS for keeping everything working over the longer term. The data presented in this paper were made possible by the long hours and hard work of E. P. Laguerta, B. C. Bautista, T. L. Murray, F. Fischer, E. P. Laguerta, L. Bautista, J. W. Ewert, A. B. Lockhart, E. Ramos, J. Power, and personnel of the U.S. Air Force at Clark Air Base. Constructive reviews by Steve Malone, and an anonymous reviewer, as well as comments from the Associate Editor Joan Gomberg helped improving the quality of this manuscript. Thanks to Chris Newhall and Mike Brudzinski for helpful discussions. This material is based upon work supported by the National Science Foundation under grant EAR-0001138.x

References

Abe, K. (1992), Seismicity of the caldera-making eruption of Mount Katmai, Alaska in 1912, *Bull. Seismol. Soc. Am.*, *82*, 175–191.

Acharya, H. K., and Y. P. Aggarwal (1980), Seismicity and tectonics of the Philippine islands, *J. Geophys. Res.*, *85*, 3239–3250.

Battaglia, J., J.-L. Got, and P. G. Okubo (2003), Location of Long-Period events below Kilauea using seismic amplitudes and accurate relative relocation, *J. Geophys. Res.*, *108*(B12), 2553, doi:10.1029/2003JB002517.

Bautista, B. C., M. L. P. Bautista, R. S. Stein, E. S. Barcelona, R. S. Punongbayan, E. P. Laguerta, A. R. Rasdas, G. Ambubuyog, and E. Q. Amin (1996), Relationship of regional and local structures of Mount Pinatubo activity, in *Fire and Mud: Eruptions and Lahars of Mount Pinatubo, Philippines*, edited by C. G. Newhall and R. S. Punongbayan, pp. 351–370, Univ. of Wash. Press, Seattle.

Brancato, A., and S. Gresta (2003), High precision relocation of microearthquakes at Mt. Etna (1991–1993 eruption onset): A tool for better understanding the volcano seismicity, *J. Volcanol. Geotherm. Res.*, *124*, 219–239.

Cardwell, R. K., B. L. Isacks, and D. E. Karig (1980), The spatial distribution of earthquakes, focal mechanism solutions, and subducted lithosphere in the Philippine and Northeastern Indonesian islands, in *Tectonic and Geologic Evolution of the Southeast Asian Seas and Islands*, *Geophys. Monogr. Ser.*, vol. 23, edited by D. E. Hayes, pp. 1–34, AGU, Washington, D. C.

Deichmann, N., and M. Garcia-Fernandez (1992), Rupture geometry from high-precision relative hypocenter locations of microearthquake clusters, *Geophys. J. Int.*, *110*, 501–517.

Delfin, F. G., Jr., H. G. Villarosa, D. B. Layugan, V. C. Clemente, M. R. Candelaria, and J. R. Ruaya (1996), Geothermal exploration of the pre-1991 Mount Pinatubo hydrothermal system, in *Fire and Mud: Eruptions and Lahars of Mount Pinatubo, Philippines*, edited by C. G. Newhall and R. S. Punongbayan, pp. 197–214, Univ. of Wash. Press, Seattle.

Everitt, B. S. (1993), *Cluster Analysis*, Edward Arnold, London.

Filson, J., T. Simkin, and L.-K. Leu (1973), Seismicity of a caldera collapse; Galapagos islands 1968, *J. Geophys. Res.*, *78*, 8591–8622.

Frémont, M.-J., and S. D. Malone (1987), High precision relative locations of earthquakes at Mount St. Helens, Washington, *J. Geophys. Res.*, *92*, 10,223–10,236.

Gillard, D., A. M. Rubin, and P. Okubo (1996), Highly concentrated seismicity caused by deformation of Kilauea's deep magma system, *Nature*, *384*, 343–346.

Got, J.-L., and P. Okubo (2003), New insights into Kilauea's volcano dynamics brought by large-scale relative relocation of microearthquakes, *J. Geophys. Res.*, *108*(B7), 2337, doi:10.1029/2002JB002060.

Got, J.-L., J. Fréchet, and F. W. Klein (1994), Deep fault plane geometry inferred from multiplet relative relocation beneath the south flank of Kilauea, *J. Geophys. Res.*, *99*, 15,375–15,386.

Hamburger, M. W., R. K. Cardwell, and B. L. Isacks (1983), Seismotectonics of the Northern Philippine island arc, in *Tectonic and Geologic Evolution of the Southeast Asian Seas and Islands: Part 2*, *Geophys. Monogr. Ser.*, vol. 27, edited by D. E. Hayes, pp. 1–21, AGU, Washington, D. C.

Harlow, D. H., J. A. Power, E. P. Laguerta, G. Ambubuyong, R. A. White, and R. P. Hoblitt (1996), Precursory seismicity and forecasting of the June 15, 1991, eruption of Mount Pinatubo, in *Fire and Mud: Eruptions and Lahars of Mount Pinatubo, Philippines*, edited by C. G. Newhall and R. S. Punongbayan, pp. 285–306, Univ. of Wash. Press, Seattle.

Hayashi, Y., and Y. Morita (2003), An image of a magma intrusion process inferred from precise hypocentral migrations of the earthquake swarm east of the Izu Peninsula, *Geophys. J. Int.*, *153*, 159–174.

Hirn, A., J.-C. Lépine, M. Sapin, and H. Delorme (1991), Episodes of pit-crater collapse documented by seismology at Piton de la Fournaise, *J. Volcanol. Geotherm. Res.*, *47*, 89–104.

Ito, A. (1985), High resolution relative hypocenters of similar earthquakes by cross-spectral analysis method, *J. Phys. Earth*, *33*, 279–294.

Jenkins, G. M., and D. G. Watts (1968), *Spectral Analysis and Its Applications*, Holden-Day, Boca Raton, Fla.

Jolly, A. D., R. A. Page, and J. A. Power (1994), Seismicity and stress in the vicinity of Mount Spurr volcano, south central Alaska, *J. Geophys. Res.*, *99*, 15,305–15,318.

Jones, J. W., and C. G. Newhall (1996), Preeruption and posteruption digital-terrain models of Mount Pinatubo, in *Fire and Mud: Eruptions and Lahars of Mount Pinatubo, Philippines*, edited by C. G. Newhall and R. S. Punongbayan, pp. 571–582, Univ. of Wash. Press, Seattle.

Klein, F. W. (1978), Hypocenter location program HYPOINVERSE, *U.S. Geol. Surv. Open File Rep., 78-694*, 113 pp.

Lee, W. H. K., and J. C. Lahr (1975), HYPO71 (revised): A computer program for determining hypocenter, magnitude, and first motion pattern of local earthquakes, *U.S. Geol. Surv. Open File Rep., 75-311*, 10 pp.

Lockhart, A. B., S. Marcial, G. Ambubuyog, E. P. Laguerta, and J. A. Power (1996), Installation, operation and technical specifications of the first Mount Pinatubo telemetered seismic network, in *Fire and Mud: Eruptions and Lahars of Mount Pinatubo, Philippines*, edited by C. G. Newhall and R. S. Punongbayan, pp. 215–223, Univ. of Wash. Press, Seattle.

Lomax, A., J. Virieux, P. Volant, and C. Berge-Thierry (2000), Probabilistic earthquake location in 3D and layered models, introduction of a metropolis-Gibbs method and comparison with linear locations, in *Advances in Seismic Event Location*, edited by C. H. Thurber and N. Rabinowitz, pp. 101–134, Kluwer Acad., Norwell, Mass.

Moran, S. (1994), Seismicity at Mount St. Helens, 1987–1992: Evidence for repressurization of an active magmatic system, *J. Geophys. Res.*, *99*, 4341–4354.

Mori, J., and C. McKee (1987), Outward-dipping ring-fault structure at Rabaul caldera as shown by earthquake locations, *Science*, *235*, 193–195.

Mori, J., D. Eberhart-Phillips, and D. H. Harlow (1996a), Three-dimensional velocity structure of Mount Pinatubo: Resolving magma bodies and earthquake hypocenters, in *Fire and Mud: Eruptions and Lahars of Mount Pinatubo, Philippines*, edited by C. G. Newhall and R. S. Punongbayan, pp. 371–382, Univ. of Wash. Press, Seattle.

Mori, J., R. A. White, D. H. Harlow, P. Okubo, J. A. Power, R. P. Hoblitt, E. P. Laguerta, A. Lanuza, and B. C. Bautista (1996b), Volcanic earthquakes following the 1991 climactic eruption of Mount Pinatubo: Strong seismicity during a waning eruption, in *Fire and Mud: Eruptions and Lahars of Mount Pinatubo, Philippines*, edited by C. G. Newhall and R. S. Punongbayan, pp. 339–350, Univ. of Wash. Press, Seattle.

Musumeci, C., S. Gresta, and S. D. Malone (2002), Magma system recharge of Mount St. Helens from precise relative hypocenter location of microearthquakes, *J. Geophys. Res.*, *107*(B10), 2264, doi:10.1029/2001JB000629.

Newhall, C. G., et al. (1996), Eruptive history of Mount Pinatubo, in *Fire and Mud: Eruptions and Lahars of Mount Pinatubo, Philippines*, edited by C. G. Newhall and R. S. Punongbayan, pp. 165–195, Univ. of Wash. Press, Seattle.

Okada, H., H. Watanabe, H. Yamashita, and I. Yokoyama (1981), Seismological significance of the 1977–1978 eruptions and magma process of Usu volcano, Hokkaido, *J. Volcanol. Geotherm. Res.*, *9*, 311–344.

Pechmann, J. C., and H. Kanamori (1982), Waveforms and spectra of preshocks and aftershocks of the 1979 Imperial Valley, California, earthquake: Evidence of fault heterogeneity?, *J. Geophys. Res.*, *87*, 10,579–10,597.

Poupinet, G., W. L. Ellsworth, and J. Fréchet (1984), Monitoring velocity variations in the crust using earthquakes doublets: An application to the Calaveras fault, California, *J. Geophys. Res.*, *89*, 5719–5731.

Power, J. A., J. C. Lahr, R. A. Page, B. A. Chouet, C. D. Stephens, D. H. Harlow, T. L. Murray, and J. N. Davies (1994), Seismic evolution of the 1989–1990 eruption sequence of Redoubt Volcano, Alaska, *J. Volcanol. Geotherm. Res.*, *62*, 69–94.

Prejean, S., W. Ellsworth, M. Zoback, and F. Waldhauser (2002), Fault structure and kinematics of the Long Valley caldera region, California, revealed by high-accuracy earthquake hypocenters and focal mechanism stress inversions, *J. Geophys. Res.*, *107*(B12), 2355, doi:10.1029/2001JB001168.

Pujol, J. (2000), Joint hypocentral location—The JHD technique and applications to data from local seismic networks, in *Advances in Seismic Event Location*, edited by C. H. Thurber and N. Rabinowitz, pp. 163–204, Kluwer Acad., Norwell, Mass.

Ratdomopurbo, A., and G. Poupinet (1995), Monitoring a temporal change of seismic activity in a volcano: Application to the 1992 eruption of Mt. Merapi (Indonesia), *Geophys. Res. Lett.*, *22*, 775–778.

Rowe, C. A., C. H. Thurber, and R. A. White (2004), Dome growth behavior at Soufriere Hills volcano, Montserrat, revealed by relocation of volcanic event swarms, 1995–1996, *J. Volcanol. Geotherm. Res.*, *134*, 199–221.

Rubin, A. M., D. Gillard, and J.-L. Got (1998), A reinterpretation of seismicity associated with the January 1983 dike intrusion at Kilauea volcano, Hawaii, *J. Geophys. Res.*, *103*, 10,003–10,015.

Rubin, A. M., D. Gillard, and J.-L. Got (1999), Streaks of microearthquakes along creeping faults, *Nature*, *400*, 635–641.

Scherbaum, F., and J. Wendler (1986), Cross spectral analysis of Swabian Jura (SW Germany) three component microearthquake recordings, *J. Geophys.*, *60*, 157–166.

Thurber, C., and D. Eberhart-Phillips (1999), Local earthquake tomography with flexible gridding, *Comput. Geosci.*, *25*, 809–818.

Toda, S., R. S. Stein, and T. Sagiya (2002), Evidence from the AD 2000 Izu islands earthquake swarm that stressing rate governs seismicity, *Nature*, *419*, 58–61.

Troise, C., G. De Natale, and F. Pingue (1997), A model for earthquake generation during unrest episode at Campi Flegrei and Rabaul calderas, *Geophys. Res. Lett.*, *24*, 1575–1578.

Waldhauser, F., and W. L. Ellsworth (2000), A double-difference earthquake location algorithm: Method and application to the northern Hayward fault, California, *Bull. Seismol. Soc. Am.*, *90*, 1353–1368.

Weaver, C. S., W. C. Grant, S. D. Malone, and E. T. Endo (1981), Post-May 18 seismicity: Volcanic and tectonic implications, *U.S. Geol. Surv. Prof. Pap.*, *1250*, 109–121.

White, R. A. (1996), Precursory deep long-period earthquakes at Mount Pinatubo: Spatio-temporal link to a basalt trigger, in *Fire and Mud: Eruptions and Lahars of Mount Pinatubo, Philippines*, edited by C. G. Newhall and R. S. Punongbayan, pp. 307–327, Univ. of Wash. Press, Seattle.

Wolfe, C. J., P. G. Okubo, and P. M. Shearer (2003), Mantle fault zone beneath Kilauea Volcano, Hawaii, *Science*, *300*, 478–480.

Wolfe, E. W., and R. P. Hoblitt (1996), Overview of the eruptions, in *Fire and Mud: Eruptions and Lahars of Mount Pinatubo, Philippines*, edited by C. G. Newhall and R. S. Punongbayan, pp. 3–20, Univ. of Wash. Press, Seattle.

Wolfe, J. A., and S. S. Self (1983), Structural lineaments and Neogene volcanism in southwestern Luzon, in *Tectonic and Geologic Evolution of the Southeast Asian Seas and Islands: Part 2*, *Geophys. Monogr. Ser.*, vol. 27, edited by D. E. Hayes, pp. 157–172, AGU, Washington, D. C.

J. Battaglia and C. H. Thurber, Department of Geology and Geophysics, University of Wisconsin–Madison, 1215 W. Dayton St., Madison, WI 53706, USA. (battag@geology.wisc.edu; clifft@geology.wisc.edu)

J.-L. Got, LGIT, Université de Savoie, F-73376 Le Bourget du Lac, France. (jean-luc.got@univ-savoie.fr)

C. A. Rowe, Los Alamos National Laboratory, EES-11 M.S. D-408, Los Alamos, NM 87545, USA. (char@lanl.gov)

R. A. White, U.S. Geological Survey, 325 Middlefield Road, Menlo Park, CA 94025, USA. (rwhite@usgs.gov)